IOPscience iopscience.iop.org

Home Search Collections Journals About Contact us My IOPscience

Structural and transport properties of GaAs/δ-Mn/GaAs/$In_xGa_{1-x}As$/GaAs quantum wells

This article has been downloaded from IOPscience. Please scroll down to see the full text article.

2008 J. Phys.: Condens. Matter 20 145207

(http://iopscience.iop.org/0953-8984/20/14/145207)

View the table of contents for this issue, or go to the journal homepage for more

Download details:
IP Address: 129.252.86.83
The article was downloaded on 29/05/2010 at 11:27

Please note that terms and conditions apply.

J. Phys.: Condens. Matter **20** (2008) 145207 (9pp) doi:10.1088/0953-8984/20/14/145207

Structural and transport properties of GaAs/δ-Mn/GaAs/$In_xGa_{1-x}As$/GaAs quantum wells

B A Aronzon[1,2], M V Kovalchuk[1], E M Pashaev[1], M A Chuev[1,3], V V Kvardakov[1], I A Subbotin[1,4], V V Rylkov[1], M A Pankov[1,2], I A Likhachev[1], B N Zvonkov[5], Yu A Danilov[5], O V Vihrova[5], A V Lashkul[6] and R Laiho[6]

[1] Russian Research Center 'Kurchatov Institute', Kurchatov Square 1, 123182 Moscow, Russia
[2] P N Lebedev Research Center in Physics, Leninskii Avenue 53, 119991 Moscow, Russia
[3] Institute of Physics and Technology of RAS, Nakhimovskii Avenue 34, 117218 Moscow, Russia
[4] A V Shubnikov Institute of Crystallography of RAS, Leninskii Avenue 59, 119333 Moscow, Russia
[5] Physico-Technical Research Institute of Nizhny Novgorod University, 603950, N Novgorod, Russia
[6] Wihuri Physical Laboratory, Department of Physics, University of Turku, FIN-20014 Turku, Finland

Received 27 November 2007, in final form 14 February 2008
Published 18 March 2008
Online at stacks.iop.org/JPhysCM/20/145207

Abstract
We report results of investigations of the structural and transport properties of GaAs/$Ga_{1-x}In_xAs$/GaAs quantum wells (QWs) having a 0.5–1.8 monolayer (ML) thick Mn layer, separated from the QW by a 3 nm thick spacer. The structure has hole mobility of about 2000 cm^2 $(V\ s)^{-1}$, being by several orders of magnitude higher than in known ferromagnetic two-dimensional (2D) structures. The analysis of the electro-physical properties of these systems is based on detailed study of their structure by means of high-resolution x-ray diffractometry and glancing-incidence reflection, which allow us to restore the depth profiles of the structural characteristics of the QWs and thin Mn-containing layers. These investigations show the absence of Mn atoms inside the QW. The quality of the structures was also characterized by photoluminescence spectra from the QWs. The transport properties reveal features inherent to ferromagnetic systems: a specific maximum in the temperature dependence of the resistance and the anomalous Hall effect (AHE) observed in samples with both 'metallic' and activated types of conductivity up to ∼100 K. AHE is most pronounced in the temperature range where the resistance maximum is observed. The results are discussed in terms of the interaction of 2D-holes and magnetic Mn ions in the presence of large-scale potential fluctuations related to the random distribution of Mn atoms. The AHE values are compared with calculations taking into account the 'intrinsic' mechanism in ferromagnetic systems.

1. Introduction

Opportunity for the creation of spintronic devices has made investigations of diluted magnetic semiconductors (DMS) one of the most active directions of current solid-state physics research [1–3]. DMS are semiconductors that contain up to 10% of magnetic impurities. There exist a number of experimental results [2, 3] on ferromagnetism and its influence on the transport of charge carriers in p-type III–V semiconductors doped with Mn. At high concentrations, up to 10^{21} cm^{-3}, Mn in these compounds has acceptor properties leading to the appearance of local magnetic moments together with free charge carriers [2, 3]. Although the microscopic mechanism of magnetic ordering in these materials is still under discussion, it is generally accepted that ferromagnetism would be mediated by free and localized holes in the impurity

 © 2008 IOP Publishing Ltd Printed in the UK

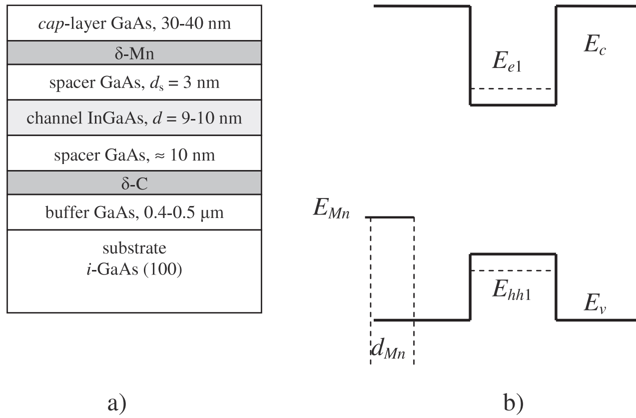

Figure 1. Configuration (a) and the band diagram (b) of the investigated samples.

band. In spite of the fact that there exist a large number of publications dedicated to (III, Mn)V DMS, investigations of two-dimensional (2D) structures are still relatively rare [4–8].

In the present work the correlation of structural and transport properties of ferromagnetic GaAs/δ-Mn/GaAs/$In_xGa_{1-x}As$/GaAs QW structures with high Mn content are investigated. In the majority of previous investigations of two-dimensional DMS showing the anomalous Hall effect, the Mn layer was located in the two-dimensional electron channel [4–7], or in spite of the spacer and rather low Mn content (0.6 ML [4]), some amount of Mn or defects had penetrated into the channel as indicated by low charge carrier mobility (2–5 cm^2 $(V\ s)^{-1}$ [4, 5]). One of the goals of the present article is to investigate the influence of Mn distribution on transport properties of the structures in which, opposite to earlier investigations, the QW and the Mn layer are well separated from each other, resulting in high carrier mobility (2000 cm^2 $(V\ s)^{-1}$), while the influence of magnetic ordering on the transport properties is still preserved. X-ray and photoluminescence (PL) studies are used to evaluate the Mn distribution and to prove a high quality of QWs free from Mn atoms. Here we report peculiarities caused by magnetic ordering in the transport properties of GaAs/δ-Mn/GaAs/$In_xGa_{1-x}As$/GaAs QW structures. The observed anomalous Hall effect conductivity is in good agreement with the theoretical predictions that the 'intrinsic' mechanism [9, 10] is the main reason for AHE in this case.

2. Samples

The samples containing an $In_xGa_{1-x}As$ QW of width d = 10 nm inside a GaAs matrix were grown by MOS-hydride epitaxy (see figure 1). The p-type conductivity in the quantum well was achieved by delta-doping using the carbon and manganese layers, which act as acceptors. The delta-layer with Mn content of about 10^{14} atoms cm^{-2} was prepared by laser deposition [8] and placed above the QW separated from it by a 3 nm thick upper spacer. The hole concentration is mainly provided by this layer. The carbon layer (about 2×10^{12} atoms cm^{-2}) was located at the buffer side of the QW and was separated from it by the 10 nm thick bottom spacer.

Table 1. Technological and physical parameters of the samples (M stands for metallic and I for activation type of conductivity).

			77 K		
Sample	x (x-ray)	d_{Mn} (ML)	μ_{eff} cm^2 $(V\ s)^{-1}$	$p\times10^{-12}$ (cm^{-2})	R_s $(\Omega/\square)$
A (M)	0.21	0.5	1860	2	1660
B (I)	0.16	1.8	1350	1.8	2540
C (I)	0.18	0	1598	0.5	7800

d_{Mn} is the effective thickness of the Mn layer; p and μ_{eff} are the concentration of holes and their effective mobility; R_s is the sample resistivity.

This layer was prepared to ensure p-type conductivity in the bottom spacer since the energy position of the QW should be close to the Fermi level, while the buffer layer had intrinsic conductivity. The buffer layer, QW, and the spacers were grown at 600 °C, while the laser deposition of the Mn and cap layers was performed at 450 °C in the same epitaxial reactor without taking the sample out of the reactor chamber. The sample parameters are given in table 1.

As shown by previous investigations [8], the optimal spacer width d_s ≈ 3 nm and there exists an optimal magnetic impurity concentration for the strongest influence of ferromagnetism on the transport properties of the 2D channel. This spacer thickness is connected, most probably, with nonzero thickness of the Mn δ-layer, since according to our previous studies at d_s < 3 nm drastic changes in the PL spectra and the activation energy of the conductivity occur, suggesting penetration of the Mn atoms into the QW. Samples with Mn atoms that penetrated or were located inside the 2D conductivity channel were investigated in [4, 5] by detecting the magnetic order with AHE. The low values of the Hall mobility of the carriers (less than 10 cm^2 $(V\ s)^{-1}$) in these cases support the statement that Mn or defects had entered the 2D channel. Both the structural investigations and the high value of the Hall mobility ≈2000 cm^2 $(V\ s)^{-1}$ at 4.2 K give evidence that in our samples the Mn ions are located outside the 2D channel. Increasing the distance of the Mn δ-layer from the QW leads to a weakening of AHE [8], i.e. of magnetic ordering because the ferromagnetism in such systems is based on carrier mediated exchange interaction.

The optimal Mn concentration in the δ-layer can be attributed to the Mn atoms at low concentration substituting for Ga and acting as acceptors, while at high concentrations (above 6 at.% in bulk samples) a considerable number of Mn atoms are located in interstitial sites playing the role of double donors [3, 11]. Also at high Mn concentrations formation of MnAs clusters is possible [12, 13], giving a considerable contribution to the magnetization of the whole structure, but not to AHE because of the Schottky barrier between the free charge carriers and the clusters [14]. This conjecture is confirmed by comparison with our previous data of magnetization and Hall measurements on samples with different contents of Mn in the δ-layer [8]. Contrary to [8], in the present structures room temperature magnetization was not observed, which indicates the absence of MnAs grains [4, 5, 11–13].

Our present samples demonstrate, depending on the growth conditions, both non-activation (quasi-metallic, sample **A**) and activation (sample **B**) types of conductivity (see section 5). For comparison, data for the sample **C**, which instead of Mn contains a carbon δ-layer, are presented.

Transport measurements were performed at $T = 4.2$–80 K in fields up to 14 T with a Hall bar sample (width $W = 0.3$ mm, distance between potential probes $L = 1.5$ mm) prepared by photolithography, while for x-ray studies samples of size 3×20 mm^2 were used.

3. High-resolution x-ray diffractometry and reflectometry

X-ray diffraction measurements of the samples were carried out at a double-crystal spectrometer using Cu Kα_1 radiation and a quasi-nondispersive scheme from [15, 16]. High quality Ge(400) and Si(111) crystals were used as collimators in the diffractometry and the reflectometry experiments, respectively. The x-ray rocking curves versus $\Delta\theta = \theta - \theta_B$ (where $\Delta\theta$ is the deviation of the incidence angle θ from the precise Bragg's angle θ_B) were measured using $\theta/2\theta$ scans with a horizontal slit positioned in front of the detector in order to minimize diffuse and background scattering. The obtained diffraction curves are shown in figure 2 with vertical dashes indicating the statistical error at each spectral point. For all samples, the intensity of the 'tails' of the rocking curve is higher at angles smaller than the exact Bragg angle for the GaAs substrate, corresponding to the larger lattice parameter of the $In_xGa_{1-x}As$ QW and giving an opportunity to estimate the In concentration (x). There are also a number of oscillations in the rocking curves, typical for high quality multilayer structures with relatively abrupt interfaces between the layers [15–18]. These interference patterns are mainly due to the coherent shift of atomic planes of the relatively thick GaAs cap layer with respect to those of the substrate, induced by the $In_xGa_{1-x}As$ QW. Such a shift results in a phase shift between the amplitudes of the diffracted waves from the cap layer and the substrate [15];

$$\Phi \propto \frac{\Delta a_\perp}{a} l_{QW}, \qquad (1)$$

where $\Delta a_\perp/a$ is the relative lattice mismatch regarding the substrate in the growth direction and l_{QW} is the thickness of the QW.

Following [18] a multilayer structure can be regarded as a system of homogeneous layers with the number of the layers not necessarily equal to that of the layers grown under the applied technological conditions. Each layer j is characterized by the thickness l_j, the lattice mismatch $\Delta a_{j\perp}/a$ and static Debye–Waller factor w_j which defines the degree of amorphism of the layer f_j, defined by the reciprocal lattice vector K and chaotic displacement u of the atoms from their regular positions into the jth sublayer

$$f_j = \exp(-w_j) = \exp(-\langle (Ku)^2 \rangle_j). \qquad (2)$$

The structural parameters were found by the conventional least-squares method using the growth parameters of the heterostructures as an initial approximation. However, a pronounced inconsistency between the experimental and the calculated rocking curves indicates that the real structures differ from those specified by the growth conditions. In order to improve the quality of fitting of the experimental rocking curves, we had to introduce additional sub-layers describing the interfaces on both sides of the QW and the natural distortions on the sample surface. The results of fitting with a seven-layer model are shown in figure 3.

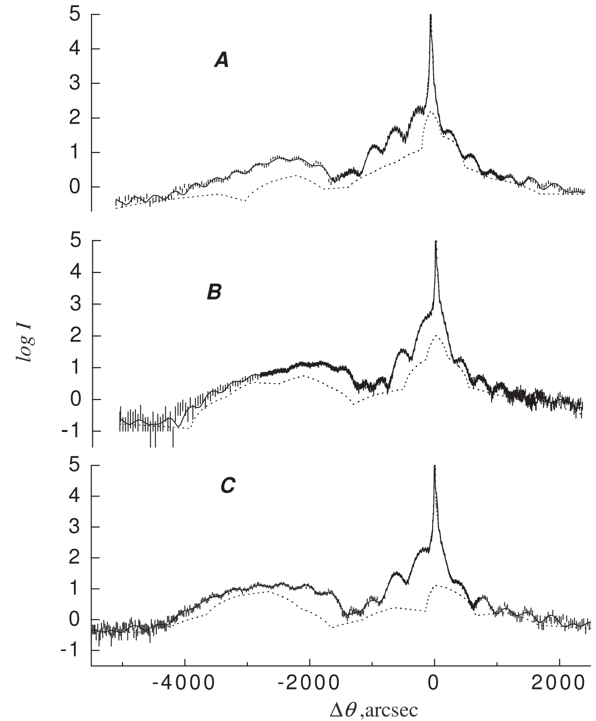

Figure 2. Experimental x-ray rocking curves taken from (004) planes of GaAs/δ-Mn/$In_xGa_{1-x}As$/GaAs (vertical dashes) and the corresponding theoretical curves (solid lines) calculated within the resulting seven-layer model ($\chi^2 = 1.45$, 1.04 and 1.15 for **A**, **B** and **C** samples, respectively). The incoherent diffuse background for each rocking curve is shown by a dotted line.

The most interesting result of the x-ray measurements is that in sample **A** the GaAs spacer between the QW and the Mn-containing layer is relatively well formed while in sample **B** this spacer prepared with practically the same technological parameters is strongly doped with Mn (figure 3). This obstacle influences the transport properties of the samples as will be shown below. The existence of a well defined δ-layer of carbon in sample **C** is questioned because such a light element as carbon is likely to diffuse into the surrounding layers.

The parameters $\Delta a_\perp/a$ and l for such thin layers are strongly correlated so that they could not be simultaneously determined with good accuracy. In particular, the rocking curve for the sample **A** as shown in figure 2 can be well fitted both within the model shown in figure 3 and a model with a 'technological' δ-Mn layer. In order to resolve the ambiguity one should apply additional methods of structural characterization.

A specific feature of our heterostructures is that the core electron density of the GaAs matrix differs from that of the

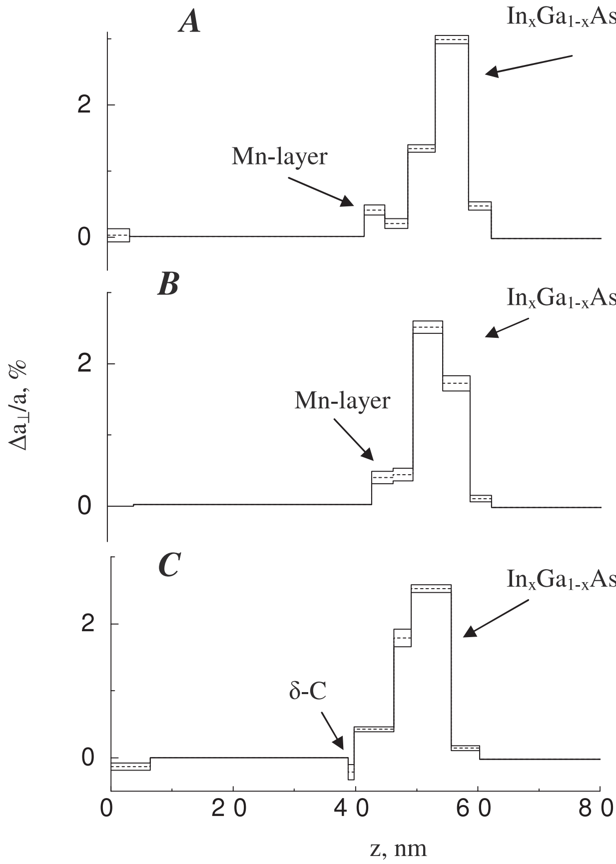

Figure 3. Depth (z) profiles of the lattice mismatch evaluated from fitting the experimental x-ray rocking curves.

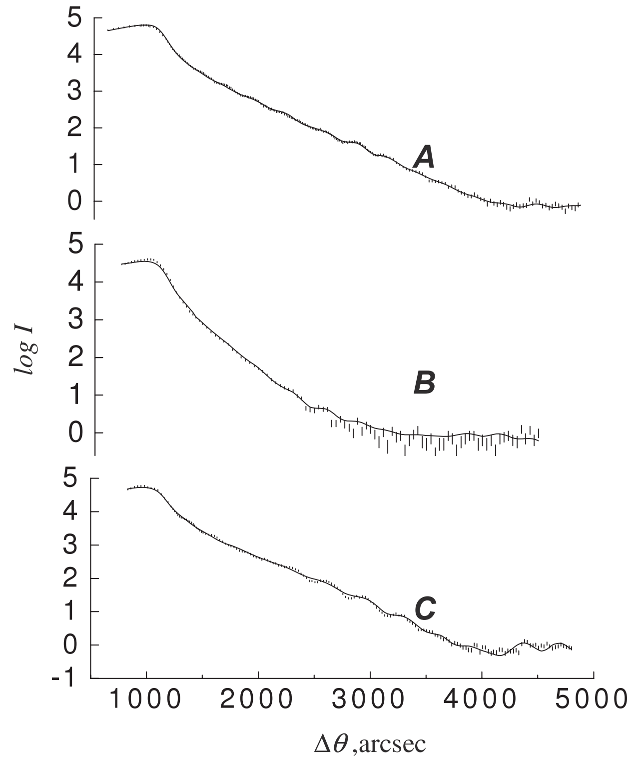

Figure 4. Experimental reflectometry curves from GaAs/δ-Mn(C)/$In_xGa_{1-x}As$/GaAs heterostructures (vertical dashes) and theoretical curves (solid lines) ($\chi^2 = 1.39$, 5.22 and 4.68 for **A**, **B** and **C** samples, respectively).

$In_xGa_{1-x}As$ QW by only a few tenths per cent while the core electron density of the Mn layer is about twice as big. Due to this fact, more detailed information about the structural characteristics of thin Mn layers can be obtained by x-ray reflectometry because the amplitude of the mirror reflection is mainly defined by the depth distribution of the core electron density. The glancing-incidence x-ray rocking curves shown in figure 4 demonstrate oscillations of the reflection intensity, although they are not so pronounced as those in the diffraction curves in figure 2.

However, the former are due mainly to a coherent shift of the atomic planes of the GaAs cap layer with respect to those of the substrate, which is defined by the thin Mn layer. The amplitude of the oscillations is proportional to the difference between the electron core densities in GaAs and Mn [19], the corresponding beats being modulated by a smoothly varying phase:

$$\Phi(\theta) \propto l_{\mathrm{Mn}}\theta, \tag{3}$$

where l_{Mn} is taken for the Mn layer thickness. These circumstances reduce the phase problem (1) for very thin layers. Even qualitative analysis of the curves in figure 4 shows that the reflectometry data can be fitted only by assuming that a thicker layer of Mn atoms is 'diluted' in GaAs but not with a 'technological' δ-Mn layer.

We have analyzed the experimental glancing-incidence x-ray rocking curves with a formalism [19] based on Parrat recursion relations for calculating the amplitude of the x-ray reflection [20] within a continuous depth distribution of the core electron density in the interfaces between the layers ($0 < z < b_j$),

$$\rho_{j+1}(z) = \rho_j + (\rho_{j+1} - \rho_j)\frac{b_j - z}{b_j}. \tag{4}$$

The detailed treatment within the least-squares procedure has allowed us to evaluate the thickness of Mn-containing layers and their interfaces as well as the relative Mn content in the layers $Mn_y(GaAs)_{1-y}$, where y is evaluated from the corresponding core electron density. We have obtained $l_{\mathrm{Mn}} = 1.9(8)$ nm, $b_{\mathrm{Mn}} = 2.1(7)$ nm, 1.7(9) nm, $y = 0.045(9)$ for sample **A** and $l_{\mathrm{Mn}} = 2.6(6)$ nm, $b_{\mathrm{Mn}} = 6.0(5)$ nm, 3.8(5) nm, $y = 0.10(2)$ for sample **B**. These values agree with those evaluated from diffraction data (figure 3) as well as allowing the total content of Mn in the layers to be estimated: these values are $d_{\mathrm{Mn}} = 0.27(5)$ ML and 1.2(4) ML for samples **A** and **B**, respectively, which qualitatively agrees with values according to the growth conditions (table 1). At the same time the results show that Mn atoms do not penetrate into the QWs of samples **A** and **B**. Note that more accurate analysis of the x-ray data requires simultaneous fitting of the diffraction and glancing-incidence x-ray rocking curves within the same model of heterostructure studied.

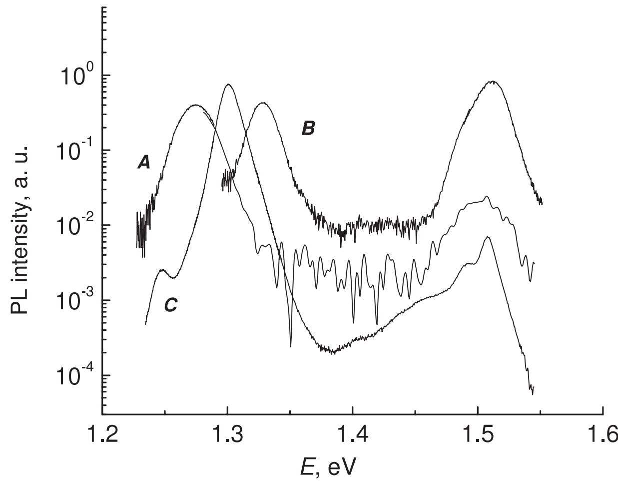

Figure 5. Photoluminescent spectra of the GaAs/δ-Mn(C)/$In_xGa_{1-x}As$/GaAs samples **A**, **B** and **C**. The maximum on the right-hand side originates from GaAs and that on the left-hand side from the QW.

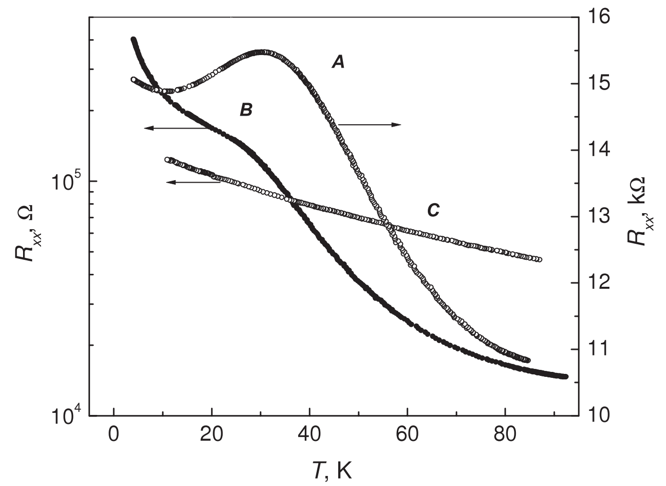

Figure 6. Temperature dependence of the resistivity for the GaAs/δ-Mn(C)/$In_xGa_{1-x}As$/GaAs samples **A**, **B** and **C**.

4. Photoluminescence

The high structural quality and absence of Mn in the QW are confirmed by the photoluminescence (PL) results presented in figure 5, taken at 77 K under illumination with a 40 mW He–Ne laser. These spectra show two maxima, the left one is related to the InGaAs QW because with increasing In content it shifts to lower energy and the right one to transitions in GaAs. The transition energies are in agreement with those calculated for the electrons (E_{e1}) and heavy holes (E_{hh1}) in the GaAs/InGaAs/GaAs QW [21]. Using the x values obtained from x-ray results (see table 1) the calculated transition energy ($E_{e1} - E_{hh1}$) is 1.25 eV for sample **A** and 1.31 eV for sample **B** in accordance with the PL results (1.27 and 1.33 eV, respectively). The difference between the observed and calculated values can be related to the fact that [21] does not take into account the stress caused by lattice mismatch. The weakening of the stress by structure distortions in the spacer layer (see figure 3) supports this consideration. However, it should be mentioned that the difference in the PL peak positions for structures A and B ($\approx$0.06 eV) coincides with the calculated value to within 0.001 eV.

Good agreement between the calculated and measured PL peak energy proves the essential role of size quantization and the 2D nature of the charge carriers. Also the PL signal from the QW has a single maximum without low energy satellites originating in the DMS from the recombination of electrons with holes bound to Mn acceptors [22], in agreement with the absence of Mn inside the QW. So, both the x-ray and PL results prove the high quality of the QW and confirm the absence of Mn atoms inside it. Also a substantial difference between the Mn distribution and spacer homogeneity is demonstrated in samples with high (**B**) and low (**A**) Mn content, resulting in sharp distinctions of their transport properties, as will be seen below.

5. Transport properties

The hole mobility $\mu_p \approx 2000$ cm^2 V^{-1}s^{-1} in our samples exceeds by more than two orders of magnitude those in the 2D $A^{III}B^{V}$ structures doped with Mn (<10 cm^2 V^{-1}s^{-1}) and where AHE was observed [4, 5]. The high values of μ_p in our samples may be connected with a good interface and the absence of Mn atoms in the conductivity channel, as shown by the x-ray and PL results. A random distribution of Mn could result in carrier localization in the fluctuation potential (FP) wells, which may be one of the reasons for the similarity of p in the **A** and **B** samples in spite of the different doping levels d_{Mn} (see table 1). The FP arising at high Mn contents will be discussed below. Sample **C** with carbon deposited instead of Mn also exhibits the activation type of conductivity. However, this is because of the very low content of carbon (about 2×10^{12} atoms cm^{-2}) which is not sufficient to screen the electric field of the surface depletion layer.

As shown in figure 6, in sample **B** with high Mn content (high amplitude of FP) the resistance R_{xx} grows exponentially upon cooling, while in sample **A** with low Mn content the resistance changes with temperature by less than 30% (curve A in figure 6). The temperature dependence of R_{xx} of sample **A** is nonexponential (activation energy is zero). This dependence is similar (except for the hump) to that in analogous structures without the Mn δ-layer and is well described by quantum corrections to conductivity [23]. This statement is supported by analysis of the magnetoresistance and the temperature dependence of the conductivity. For simplicity we will refer to sample **A** as having quasi-metallic conductivity.

The random distribution of the charged Mn ions both in the sample plane and along the thickness of the structures can give rise to FP. One of the main reasons for FP is the compensation accompanying high levels of doping [24], another is the fluctuation of the Mn layer thickness which results in fluctuations of the effective spacing between the Mn layer and the QW. In the frame of the FP model, the unexpected transition from quasi-metallic (**A**) to activation temperature dependence of conductivity (**B**) with increasing doping could

be naturally explained. The reason is that the fluctuation potential will show itself in sample **B** with higher Mn content more distinctly than in sample **A**, leading to the carrier localization. It is clear from the x-ray measurements (figure 3) that fluctuation of the Mn layer thickness (penetration of Mn atoms inside the spacer) is much stronger in sample **B** than in **A**.

The compensation level in sample **B** is also higher than in **A** because above certain concentrations (6 at.% in bulk, unannealed samples [11–13]) the Mn atoms enter interstitial states rather than Ga positions [3]. That gives rise to compensation because the Mn ions substituting for Ga act as acceptors and those occupying the interstitial sites act as double donors [3, 11, 12]. The total concentration of the charged impurities, $N = N_A^+ + N_D^-$, strongly exceeds that of the carriers, $p = N_A^+ - N_D^-$, which cannot screen random spatial fluctuations of charge $\sim N^{1/2}$. Here N_D and N_A are the concentrations of the donors and the acceptors, respectively. The unscreened charge gives rise to long-range FP [24]. So both reasons for FP tend to localize the carriers in the FP wells, resulting in the activation character of the conductivity in sample **B**.

The theory of the FP related to compensation (sample **B**) is well developed for 2D nonmagnetic structures [25], following the known results for 3D systems [24]. In particular, the case of a highly charged impurity concentration ($N \gg a_B^{-2}$) close to the conductivity channel when $d_s < a_B$ was studied, where d_s is the thickness of the spacer between the conductivity channel and the plane of the doping layer and a_B is the Bohr radius. This is just the case for our samples where $a_B \approx 6$ nm, $d_s \leqslant 3$ nm. The energy difference between the percolation level and the Fermi energy is about the mean square amplitude of the FP wells [25]

$$\gamma = \beta \frac{e^2}{\kappa} N^{1/2} \ln^{1/2} \frac{N^{3/4}}{p a_B^{1/2}} = \beta \frac{e^2}{\kappa} R_c p \ln^{1/2} \left(\frac{R_c^3 p}{a_B} \right)^{1/2}, \quad (5)$$

where β is a factor of about 1, κ is the permittivity and $R_c = N^{1/2}/p$ is the screening length which characterizes the FP scale [25]. The concentration N of the charged impurities is not well known and usually is much lower than the concentration of introduced Mn impurities [26, 27]. Therefore, it is more instructive to use the relation $R_c = N^{1/2}/p$ and express γ in terms of R_c and p—parameters which could be found from the experimental data (see below).

From equation (5) it follows that γ does not depend on d_s for sample **B**. This is due to the dependence of the Coulomb energy not only on the distance between the Mn δ-layer and the QW but also on the characteristic size of the carrier wavefunction and the d_s value is not important if $d_s < a_B, d$. Here d is the QW thickness. So, at first glance the fluctuations of the Mn layer thickness, which could be treated as fluctuations of the effective spacer thickness, do not affect the energy of the carriers in the FP wells. However in our case d_s is less but comparable with a_B and d and one should take into account the penetration of Mn atoms inside the spacer (see figure 3) as an additional reason for the FP. This statement is reinforced by the existence of structural defects and interface

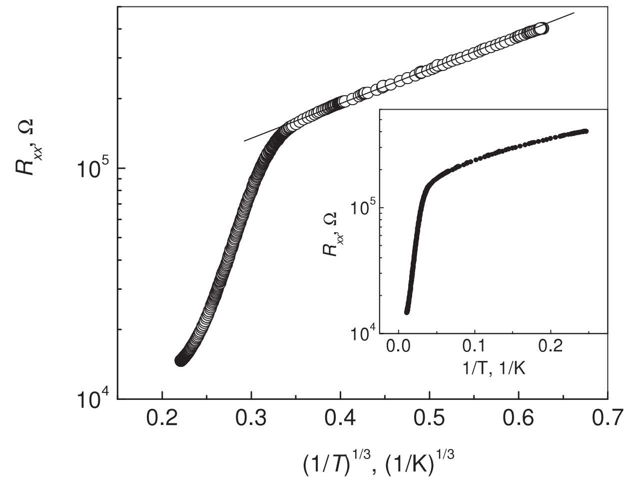

Figure 7. Temperature dependence of the resistance of sample **B**. The inset shows the resistance versus $1/T$. At low temperatures $1/T^{1/3}$ provides better fitting than $1/T$, while at higher temperatures the situation is quite the opposite.

roughness caused by Mn in the spacer (see figure 3). However, having no other theoretical results, we will use equation (5) for a rough evaluation of the FP parameters.

The charged carriers are localized at the minima of the fluctuation potential where they have high densities forming 'metallic' droplets. We call them metallic because of the long-range nature of FP; when the size of the potential well exceeds the mean free path of the holes they can act as free carriers. At the same time the Mn concentration in these regions is above average. Both the high densities of carriers and of Mn impurities promote magnetic ordering and possible local ferromagnetic transition in these areas [28] since the ferromagnetic ordering is expected to be mediated by carriers [3]. As a result, the sample contains conductive regions ('metallic droplets or lakes'), which could be ferromagnetic at low enough temperatures.

The metallic droplets may form a continuous percolation cluster resulting in quasi-metallic conductivity (sample **A**). In the case of separated metallic droplets activation type conductivity is observed (sample **B**). The activation character of sample **B** conductivity is shown in the inset to figure 7. At $T > T_t = 24$ K the $R_{xx}(T)$ dependence is determined by carrier activation over the percolation level with the activation energy $\varepsilon_a = 10.5$ meV and at $T = T_t$ there is a crossover to 2D hopping conductivity with $\ln R_{xx} \propto (1/T)^{1/3}$ (figure 7). This is in accordance with the theoretical results for transport in FP [25].

The crossover temperature from activated conductivity of the carriers to tunneling between the FP wells can be used for estimation of the characteristic size of the potential well and the radius R_c of the metallic droplets [25]. Following [25] the energy gap between the percolation level and the Fermi level is roughly equal to the amplitude of the fluctuating potential, $\gamma \approx \varepsilon_a = 10.5$ meV. For estimation of R_c we compare the probability of activation of the holes to the percolation level, $w_a \sim \exp(-\gamma/kT)$, with the probability of tunneling between the hole droplets, $w_t \sim \exp(-2R_c/\lambda)$, where $\lambda =$

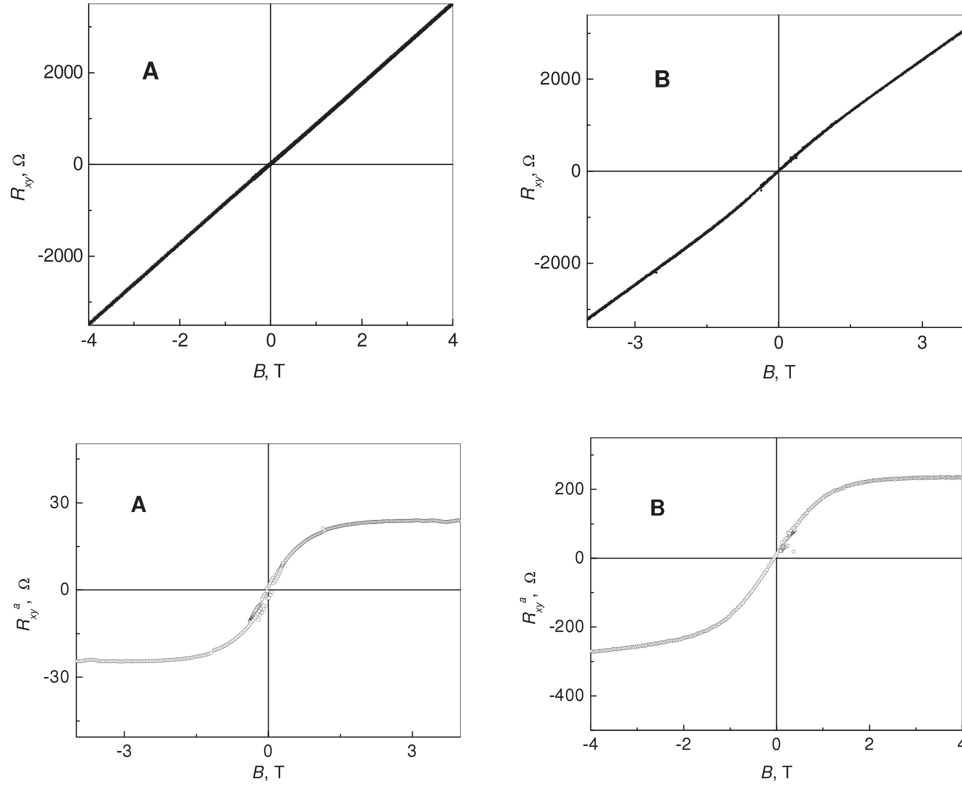

Figure 8. Magnetic field dependences of R^n_{xy} (upper panels) and of R^a_{xy} (lower panels) for samples **A** ($T = 17$ K) and **B** ($T = 55$ K). The value of the anomalous component was obtained by deduction of the normal Hall component estimated in fields up to 15 T from the total Hall response.

$\hbar/(2m^*\gamma)^{1/2}$ is the decay length of the wavefunction under the barrier of height defined by the energy difference between the percolation and the Fermi levels [25]. Taking into account that crossover takes place at $T = T_t = 24$ K one gets $R_c \approx 20$ nm, which is longer than the mean free path of the holes l_h. At $\mu \approx 10^3$ cm^2 V^{-1} s^{-1} and $T \approx 30$ K we get $l_h \approx 6$ nm. Using the obtained value $R_c \approx 20$ nm and the hole concentration $p \sim 10^{12}$ cm^{-2} on the base of equation (5) one can estimate $\gamma \sim 10$–20 meV, which is in agreement with $\varepsilon_a = 10.5$ meV.

The main peculiarity of the data in figure 6 is the maximum of $R_{xx}(T)$ observed in samples **A** and **B** at about 30–40 K, but not in the carbon-containing sample **C**. The existence of a maximum in $R_{xx}(T)$ is common for 3D and 2D DMS structures and ferromagnetic metals as well [4, 12]. This feature is often used for estimation of the Curie temperature [3, 4, 12], even in the case of an activation type conductivity [29]. Accordingly this gives in our samples a value of $T_c \approx 30$–40 K. An exact description of the resistivity hump in DMS is under discussion and several models have been suggested, taking into account the scattering of carriers by critical fluctuations close to the ferromagnetic transition, the splitting of the hole spin subbands and so on [3, 12]. In highly disordered materials the peculiarities of $R_{xx}(T)$ at $T = T_c$ could be caused by phase separation and carrier scattering by magnetic clusters [30, 31]. Analogous effects could take place in our case when the holes are scattered by magnetic moments of the metallic droplets and/or due to increasing size of the droplets with lowering of the temperature [28].

More detailed information on magnetic properties, in particular on T_c, can be obtain by measurements of AHE [3, 4, 12]. The fluctuating model featured above helps us to understand the details of AHE presented in figure 8. Nonlinearity of the Hall resistance is typical for ferromagnetic materials where the Hall voltage is a sum of normal and anomalous contributions and the Hall resistance

$$R_{xy} = \frac{\rho_{xy}}{d} = R^n_{xy} + R^a_{xy} = \frac{R_0}{d}B + \frac{R_s}{d}M, \quad (6)$$

where d is the thickness of the conducting channel (QW in our case), R^n_{xy} and R^a_{xy} are normal and anomalous contributions to the Hall resistance, while R_0 is the constant of the normal Hall effect and R_s is the AHE constant caused by the spin–orbital interaction of carriers and is related to exchange splitting of the spin sub-bands of the holes, which is proportional to the magnetization M. AHE arises from the interaction between charge carriers and the magnetic subsystem and could be significant up to (2–3) T_c [11, 12].

In 2D structures measurement of AHE is an effective method for studying magnetic ordering, because small values of M cannot be extracted by magnetometer measurements due to a large diamagnetic contribution from the substrate [4, 7]. In our case, the normal component R^n_{xy} in equations (6) strongly predominates and special efforts are needed to extract the AHE component. We determined R^n_{xy} in a high magnetic field, taking into account that contrary to the AHE this component is not saturated in magnetic fields. The results are presented

in figure 8. The data for sample **A** are given at $T = 17$ K, because at higher temperatures the ratio $R^{\mathrm{a}}_{xy}/R^{\mathrm{n}}_{xy} = \rho^{\mathrm{a}}_{xy}/\rho^{\mathrm{n}}_{xy}$ is too small. It should be emphasized that this is the first observation of AHE in 2D DMS structures with high carrier mobility. The small value of $\rho^{\mathrm{a}}_{xy}/\rho^{\mathrm{n}}_{xy}$ is not due to the small AHE conductivity, σ^{a}_{xy}, but is due to the high value of the normal component of the Hall effect, σ^{n}_{xy}.

The values of the anomalous and the normal Hall conductivities are

$$\sigma^{a}_{xy} = \rho^{\mathrm{a}}_{xy}/\rho^{2}_{xx} \qquad \text{and} \qquad \sigma^{n}_{xy} = \rho^{\mathrm{n}}_{xy}/\rho^{2}_{xx}. \qquad (7)$$

In a not too strong magnetic field we have $\sigma^{n}_{xy} = \frac{pe^2}{m^*}\omega_{\mathrm{c}}(\frac{\tau^2}{1+\omega_{\mathrm{c}}^2\tau^2}) \propto \tau^2$ assuming that $\omega_{\mathrm{c}}\tau < 1$. Here m^* is the hole effective mass, τ is the momentum relaxation time and $\omega_{\mathrm{c}} = \frac{eB}{m^*c}$ is the cyclotron frequency. On the other hand, according to recent theoretical results the main mechanism contributing to AHE in DMS and, particularly, in magnetic 2D structures [9, 10] is 'intrinsic' or nondissipative [3, 32, 33], meaning that σ^{a}_{xy} does not depend on scattering rate. So, as follows from (7), the ratio $\rho^{\mathrm{a}}_{xy}/\rho^{\mathrm{n}}_{xy} = \sigma^{a}_{xy}/\sigma^{n}_{xy} \propto \tau^{-2}$ and the contribution of AHE to the signal is higher at lower carrier mobility. That is why AHE in 2D DMS structures had so far only been observed in structures with very low carrier mobility. This is the reason why R^{a}_{xy} for sample **B** is considerably smaller than that measured by Nazmul *et al* [4] in similar structures with mobility about two orders of magnitude less. At low temperatures the carrier mobility in samples **A** is several times greater than in **B** and R^{a}_{xy} is correspondingly smaller (see figure 8), while σ^{a}_{xy} is of the same order of magnitude.

Finally, we get $\sigma^{a}_{xy} \cong 0.07e^2/h$ for sample **A** and $\sigma^{a}_{xy} \cong 0.17e^2/h$ for sample **B**. The difference between these values correlates with different Mn content (see table 1) and the depth of Mn penetration into the spacer in **A** and **B** (see figure 3). From the recent theoretical calculations of AHE in 2D structures [9, 10] one can obtain $\sigma^{a}_{xy} \sim 0.1e^2/h$ in accordance with the measured values. So the experimental results support the theoretical prediction that the 'intrinsic' mechanism is the main reason for AHE in our samples. Additional support for this could be obtained by comparison of the theoretical and experimental results for the dependence $R^{\mathrm{a}}_{xy}(\rho_{xx})$. For an 'intrinsic' mechanism $R^{\mathrm{a}}_{xy} \propto \rho^{2}_{xx}$, which is just what we have found for sample **B** using the temperature as the parameter (inset in figure 9). Of course, this result is valid only at high enough temperatures, when the conductivity is determined by the carriers activated above the percolation level but not by the hopping mechanism.

It is widely accepted that observation of AHE is the main tool for detecting magnetic ordering in DMS [3], especially in 2D structures where bulk magnetization measurements are difficult. The present results provide evidence of magnetic ordering and hole mediated coupling between local Mn moments in our samples, in accordance with theoretical calculations [9, 10] of AHE in 2D DMS structures assuming substantial spin polarization of the carriers. So we can conclude that very likely the carriers in our samples are spin polarized, as is also supported by observations of photoluminescence polarization in similar structures [34].

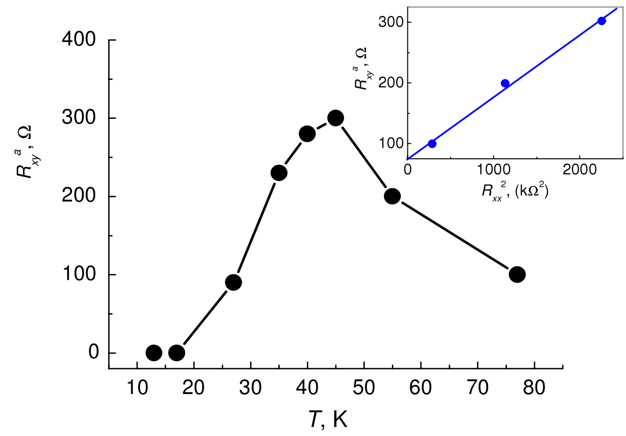

Figure 9. The temperature dependence of the anomalous Hall resistance R^{a}_{xy} for sample **B**. The inset demonstrates the parametric dependence between R^{a}_{xy} and R_{xx}.

(This figure is in colour only in the electronic version)

However, to prove this model finally the photoluminescence polarization measurements in these particular samples are needed.

The temperature dependence of R^{a}_{xy} suggests that AHE can be observed for sample **B** up to $T^{*}_{\mathrm{m}} \geqslant 80$ K, which agrees with the value $T_{\mathrm{m}} \approx 70$–100 K below which the resistivity starts to grow (see figure 6). Because the AHE and the magnetic moment should be measurable below $T \approx$ (2–3) T_{c} [11, 12] we get $T_{\mathrm{c}} \approx 30$–35 K in agreement with the temperature of the $R_{xx}(T)$ maximum. According to the FP model, T_{c} is probably related to local ferromagnetic transitions inside the metallic hole droplets. Below 40 K the value of R^{a}_{xy} for sample **B** surprisingly drops. The reason for this is the crossover to hopping conductivity with lowering of the temperature. It should be noted that at a first approximation the hopping conductivity does not contribute to the Hall effect. So AHE drops with diminishing of the activated transport, as can be observed from figure 9.

As shown in figure 8 the magnetic field dependence of R^{a}_{xy} for sample **A** gives some hints for the existence of a hysteresis loop. However, the small signal to noise ratio prevents us from making any strong conclusions. On the other hand, the hysteresis loop should be weakened because the anisotropy of the sample tends to align the magnetic moment along the plane of the structure, diminishing the Hall effect around zero magnetic field.

6. Conclusions

As a result of versatile investigations, we have observed a strong correlation between structural, electronic and optical properties in 2D GaAs/$Ga_{1-x}In_xAs$/GaAs QWs containing an Mn δ-layer. With x-ray diffractometry and reflectometry measurements precise distributions of the lattice parameters of the QWs and the Mn δ-layers are obtained. The structural investigations confirm the absence of Mn atoms inside the QW. The quality of the sample structures is characterized also by

photoluminescence spectra showing emission lines from the QWs in good agreement with x-ray measurements.

Although there should be no Mn atoms inside the QW, the presence of AHE and the maximum in the temperature dependence of the resistivity component R_{xx} at 35 K give evidence for magnetic ordering in samples **A** and **B**. As a result, the AHE is observed for the first time in a 2D DMS structure with high mobility of the holes (2000 $cm^2 V^{-1} s^{-1}$). The values of σ_{xy}^a agree reasonably with theoretical predictions [9, 10] in corresponding structures in the presence of spin polarized carriers. The agreement between the measured and calculated values of σ_{xy}^a and the observed $R_{xy}^a \propto \rho_{xx}^2$ dependence are symptoms of 'intrinsic' AHE in our samples. The σ_{xy}^a values also correlate with the Mn content of the samples.

The low temperature conductivity at high Mn content (1.5 ML) is determined by hopping of carriers localized in the wells of long-range fluctuating Coulomb potential. The amplitude and the scale of the fluctuations are estimated from the temperature dependence of the resistivity with the result that the size of the potential wells noticeably exceeds the mean free path of the holes. With lowering of the temperature, AHE reaches a maximum at $T = T_c$ and diminishes with further decrease of the temperature.

Acknowledgments

The authors are grateful to K I Kugel and E Z Meilikhov for fruitful discussions, and to ISTC (grant G1335), RFBR (grants 07-02-00927, 08-02-00719, 08-02-01462) and the Wihuri foundation for support.

References

[1] Žutić I, Fabian J and Das Sarma S 2004 *Rev. Mod. Phys.* **76** 323
Zakharchenya B P and Korenev V L 2005 *Phys.—Usp.* **48** 603
[2] Dietl T, Ohno H and Matsukura F 2001 *Phys. Rev.* B **63** 195205
Ohno H 2001 *Science* **291** 840
[3] Jungwirth T, Sinova J, Mašek J, Kučera J and MacDonald A H 2006 *Rev. Mod. Phys.* **78** 809
[4] Nazmul A M, Sugahara S and Tanaka M 2003 *Phys. Rev.* B **67** 241308
Nazmul A M, Amemiya T, Shuto Y, Sugahara S and Tanaka M 2005 *Phys. Rev. Lett.* **95** 017201
[5] Wojtowicz T, Lim W L, Liu X, Dobrowolska M, Furdyna J K, Yu K M, Walukiewicz W, Vurgaftman I and Meyer J R 2003 *Appl. Phys. Lett.* **83** 4220
[6] Luo H, Kim G B, Cheon M, Chen X, Na M, Wang S, McCombe B D, Liu X, Sasaki Y, Wojtowicz T, Furdyna J K, Boishin G and Whitman L J 2004 *Physica* E **20** 338
[7] Ohno H, Chiba D, Matsukura F, Omiya T, Abe E, Dietl T, Ohno Y and Ohtani K 2000 *Nature* **408** 944
Matsukura F, Chiba D, Omiya T, Abe E, Dietl T, Ohno Y, Ohtani K and Ohno H 2002 *Physica* E **12** 351
[8] Aronzon B A, Granovsky A B, Davydov A B, Danilov Yu A, Zvonkov B N, Ryl'kov V V and Uskova E A 2007 *Phys. Solid State* **49** 171
[9] Liu S Y and Lei X L 2005 *Phys. Rev.* B **72** 195329
[10] Dugaev V K, Bruno P, Taillefumier M, Canals B and Lacroix C 2005 *Phys. Rev.* B **71** 224423
[11] Edmonds K W, Wang K Y, Campion R P, Neumann A C, Foxon C T, Gallagher B L and Main P C 2002 *Appl. Phys. Lett.* **81** 3010
Edmonds K W, Bogusławski P, Wang K Y, Campion R P, Novikov S N, Farley N R S, Gallagher B L, Foxon C T, Sawicki M, Dietl T, Nardelli M B and Bernholc J 2004 *Phys. Rev. Lett.* **92** 037201
[12] Ohno H and Matsukura F 2001 *Solid State Commun.* **117** 179
[13] Ohno H 1999 *J. Magn. Magn. Mater.* **200** 110
Mahadevan P and Zunger A 2003 *Phys. Rev.* B **68** 075202
[14] Rylkov V V, Aronzon B A, Danilov Yu A, Drozdov Yu N, Lesnikov V P, Maslakov K I and Podol'ski V V 2005 *JETP* **100** 742
[15] Afanas'ev A M, Chuev M A, Imamov R M, Pashaev E M, Yakunin S N and Horvat J 2001 *JETP Lett.* **74** 498
[16] Yakunin S N, Pashaev E M, Zaitsev A A, Subbotin I A, Rzaev M M and Imamov R M 2005 *Russian Microelectron.* **34** 242
[17] Pashaev E M, Yakunin S N, Zaitsev A A, Mokerov V G, Fedorov Yu V, Horvat Zs J and Imamov R M 2003 *Phys. Status Solidi* a **195** 204
[18] Chuev M A, Afanas'ev A M, Imamov R M, Mukhamedzhanov E Kh, Pashaev E M and Yakunin S N 2004 *Proc. SPIE Micro-and Nanoelectronics* **5401** 543
[19] Chuev M A, Subbotin I A, Pashaev E M, Kvardakov V V and Aronzon B A 2007 *JETP Lett.* **85** 17
[20] Parratt L G 1954 *Phys. Rev.* **95** 359
[21] Calculation of ground energy of electron and hole in quantum wells were performed with the help of the program presented at http://www.ioffe.ru/?row=12&subrow=0#
[22] Sapega V F, Ramsteiner M, Brandt O, Däweritz L and Ploog K H 2006 *Phys. Rev.* B **73** 235208
[23] Minkov G M, Germanenko A V, Rut O E, Sherstobitov A A and Zvonkov B N 2007 *Phys. Rev.* B **75** 193311
[24] Shklovskii B I and Efros A L 1984 *Electronic Properties of Doped Semiconductors* (Berlin: Springer)
[25] Gergel' V A and Suris R A 1978 *JETP* **75** 191
[26] May S J, Blattner A J and Wessels B W 2004 *Phys. Rev.* B **70** 073303
[27] Jungwirth T, Wang K Y, Masek J, Edmonds K W, Konig J, Sinova J, Polini M, Goncharuk N A, MacDonald A H, Sawicki M, Rushforth A W, Campion R P, Zhao L X, Foxon C T and Gallagher B L 2005 *Phys. Rev.* B **72** 165204
[28] Caprara S, Chumakov N K, Gudenko S and Tugushev V 2006 *Phys. Rev.* B **74** 104204
[29] Yuldashev Sh U, Jeon H C, Im H S, Kang T W, Lee S H and Furdyna J K 2004 *Phys. Rev.* B **70** 193203
[30] Alvarez G and Dagotto E 2003 *Phys. Rev.* B **68** 045202
[31] Kagan M Yu, Kugel K I, Rakhmanov A L and Pazhitnykh K S 2006 *J. Phys.: Condens. Matter* **18** 10905
[32] Jungwirth T, Niu Q and MacDonald A H 2002 *Phys. Rev. Lett.* **88** 207208
[33] Dietl T, Matsukura F, Ohno H, Cibert J and Ferrand D 2003 *Recent Trends in Theory of Physical Phenomema in High Magnetic Fields* ed I Vagner (Dordrecht: Kluwer) p 197 (*Preprint* cond-mat/0306484)
[34] Kulakovskii V D 2007 private communication